NANO LETTERS

XXXX
Vol. xx, No. x
-

p-Type ZnO Nanowire Arrays

G. D. Yuan,[†] W. J. Zhang,*[,†] J. S. Jie,[†] X. Fan,[†,‡] J. A. Zapien,[†] Y. H. Leung,[†] L. B. Luo,[†] P. F. Wang,[‡] C. S. Lee,[†] and S. T. Lee*[,†]

Centre Of Super-Diamond and Advanced Films (COSDAF) and Department of Physics and Materials Science, City University of Hong Kong, Hong Kong SAR, People's Republic of China, and Nano-organic Photoelectronic Laboratory, Technical Institute of Physics and Chemistry, Chinese Academy of Sciences, Beijing 100080, China

Received November 19, 2007; Revised Manuscript Received April 9, 2008

ABSTRACT

Well-aligned ZnO nanowire (NW) arrays with durable and reproducible p-type conductivity were synthesized on α-sapphire substrates by using N_2O as a dopant source via vapor−liquid−solid growth. The nitrogen-doped ZnO NWs are single-crystalline and grown predominantly along the [110] direction, in contrast to the [001] direction of undoped ZnO NWs. Electrical transport measurements reveal that the nondoped ZnO NWs exhibit n-type conductivity, whereas the nitrogen-doped ZnO NWs show compensated highly resistive n-type and finally p-type conductivity upon increasing N_2O ratio in the reaction atmosphere. The electrical properties of p-type ZnO NWs are stable and reproducible with a hole concentration of $(1-2) \times 10^{18}$ cm^{-3} and a field-effect mobility of 10−17 cm^2 V^{-2} s^{-1}. Surface adsorptions have a significant effect on the transport properties of NWs. Temperature-dependent PL spectra of N-doped ZnO NWs show acceptor-bound-exciton emission, which corroborates the p-type conductivity. The realization of p-type ZnO NWs with durable and controlled transport properties is important for fabrication of nanoscale electronic and optoelectronic devices.

One-Dimensional (1D) semiconductor nanostructures, for example, nanowires,[1–6] nanotubes,[7,8] and nanoribbons,[9,10] are promising building blocks for nanoelectronic and nano-optoelectronic devices, such as light-emitting diodes (LEDs),[11–14] photodiodes,[15] and other integrated systems.[16–20] For such applications, realization of predictable and reproducible electronic properties in 1D nanostructures is a critical prerequisite. Success in controlled doping and assembly of semiconductor NWs has enabled the realization of novel circuit concepts, such as 3D integrated electronics,[17] heterostructure-based multicolor LEDs,[11] nanoscale avalanche photodetectors,[15,21] nano solar cells,[22] and nano address decoders.[19]

Doping for n- and p-type conduction has been achieved in semiconductor nanowires, such as Si,[21–23] Ge,[24] In_2O_3,[25] InP,[26,27] and GaN,[28–32] via various approaches, such as in situ doping during growth,[21–24,26–32] postannealing,[33] and ion implantation,[25,34] although each technique has inherent problems. For example, postannealing frequently leads a severe decrease in near-band-edge (NBE) emission intensity due to dopant contamination on nanowire surfaces.[33] Ion implantation invariably induces high-density defects/damage, causing a deleterious effect on crystal structure and high resistivity in NWs.[25] Also, it is difficult to achieve controlled doping and electrical properties in NWs via postannealing and ion implantation. By comparison, the in situ doping approach is much better and can realize reliable and controlled doping profile via judicious control of growth parameters while keeping the nanostructure intact.[26–32]

ZnO nanostructures have attracted intense interest as an important II−VI semiconductor with extensive application potentials. As-grown ZnO nanostructures typically show n-type conductivity due to intrinsic defects, while group III elements such as Al, Ga, and In are commonly used as dopants for n-type conductivity in ZnO nanostructures.[32–41] In contrast to n-type doping, p-type doping of ZnO nanostructures has been difficult and rarely achieved. Recently, p-type conduction was reported in ZnO nanowire arrays grown using P_2O_5 as dopan;[42] however, such p-type conduction was unstable and changed to n-type after 2 months of storage in air ambient. The instability is probably due to the larger atomic size of phosphorus than oxygen. Unlike the thin-film counterpart,[42–44] controlled doping in 1D ZnO nanomaterials remains a challenge to overcome.

Nitrogen, with an atomic radius similar to oxygen, 0.75 vs 0.73 Å, should be a better candidate than phosphorus as p-type dopant in ZnO NWs.[37] Further, a gaseous dopant source should be better than a solid one in terms of controllability and effectiveness. Guided by these expectations, we achieve the production of p-type conduction in well-aligned ZnO NWs by using N_2O as a dopant source. Further, we demonstrate that nitrogen doping can affect the growth direction of NWs. Gate-dependent $I-V$ measurements

* Corresponding authors, apwjzh@cityu.edu.hk (Zhang) and apannale@cityu.edu.hk (Lee).
[†] City University of Hong Kong.
[‡] Technical Institute of Physics and Chemistry, Chinese Academy of Sciences.

10.1021/nl073022t CCC: $40.75
Published on Web 07/12/2008

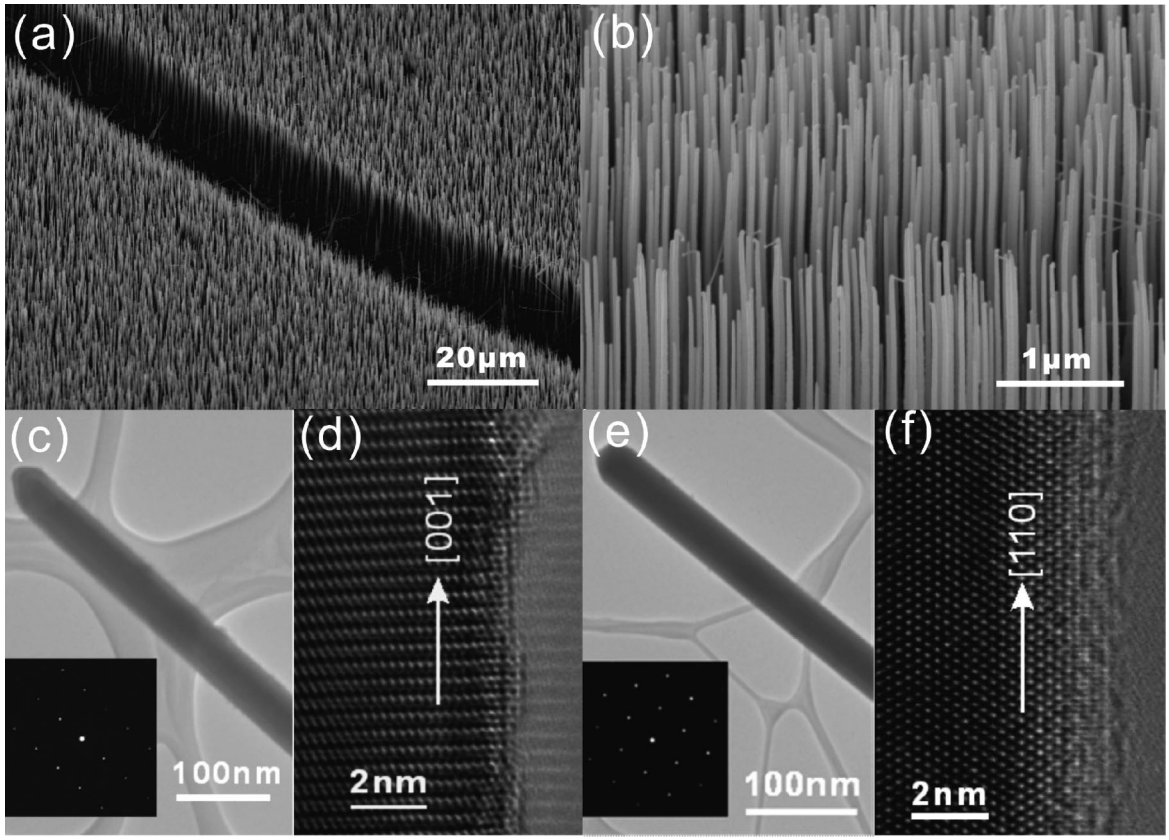

Figure 1. Morphological and structural characterization of the undoped and nitrogen-doped ZnO NWs. (a, b) SEM images of the undoped and the nitrogen-doped ZnO NWs, respectively. (c) Low-resolution TEM and SAED (inset) of undoped ZnO NWs. (d) High-resolution TEM of undoped ZnO NWs. (e) Low-resolution TEM and SAED (inset) of nitrogen-doped ZnO NWs. (f) High-resolution TEM of nitrogen-doped ZnO NWs.

of single-NW field effect transistors (FETs) show that the electrical properties of ZnO NWs could be tuned by nitrogen doping. Moreover, surface adsorption was found to have a significant effect on the transport properties of NWs.

The undoped and nitrogen-doped ZnO NWs were grown via a simple chemical vapor deposition (CVD) method using a 1:1 molar mixture of ZnO and graphite powder as the source material, and 60% argon and 20% oxygen at 200 sccm as the carrier and reactive gases, respectively. N_2O was added to the reaction atmosphere to synthesize nitrogen-doped ZnO NWs. The mixed powder source was loaded inside a tungsten crucible coated with alumina. α-Plane sapphire substrates were cleaned using a standard wafer cleaning procedure and then coated with a thin gold layer as the catalyst. The Au-coated sapphire was set at a fixed distance (about 0.5−1.5 cm) above the crucible. During experiments, the substrate and the source mixture were heated to about 750 and 950 °C, respectively. Pressure in the reaction chamber was maintained at 150 Torr, and the growth duration was 15−30 min. ZnO NWs were characterized with scanning electron microscopy (SEM, Philips XL 30 FEG) and high-resolution transmission electron microscopy (HRTEM, Philips CM200 FEG operated at 200 kV). Temperature-dependent photoluminescence (PL) measurements were conducted by using a Nd:YAG laser with a wavelength of 266 nm and a pulse width of 6 ns as the excitation source.

ZnO NWs synthesized with N_2O:O_2:Ar_2 ratios of 0:20:60, 1:20:60, and 2:20:60, are denoted as samples A, B, and C, respectively. Both undoped (sample A) and nitrogen-doped (sample B and C) ZnO NW arrays are gray in color. As shown in panels a and b of Figure 1, in all the samples (undoped and nitrogen-doped) NWs are vertically aligned on the sapphire substrates and only grown at the Au-coated area. After 15 min of growth, ZnO NWs have a uniform diameter of 70−90 nm and a wire length about 20 μm. Figure 1c shows the typical TEM image of a NW in sample A, and the selected-area electron diffraction (SAED) pattern (inset) reveals the [001] growth direction of the NW. A typical HRTEM image of the NW of sample A in Figure 1d shows a lattice distance of 0.52 nm, which coincides with the lattice spacing of (001) ZnO planes. The [001] growth direction was also confirmed by X-ray diffraction (XRD) measurements of the bulk sample.

Although the NWs in nitrogen-doped sample B are also aligned vertically on the substrate (Figure 1b), TEM and SAED observations show the nitrogen-doped NWs grow instead along the [110] direction (Figure 1, panels e and f), in sharp contrast to the undoped NWs (Figure 1, panels c and d). The XRD pattern of sample B (not shown here) shows almost exclusively the (110) diffraction peak of ZnO, confirming the TEM observations. Similar to sample B, nitrogen-doped sample C also shows the same growth

direction of [110]. Such orientation changes were verified by HRTEM and XRD examination of over 20 NWs in every sample. It confirms definitively and significantly that the growth direction of ZnO NWs can indeed be changed by introducing N_2O into the reaction atmosphere.

ZnO nanowire arrays grown on α-sapphire substrates generally have a growth direction along [001] orientation, in accordance with the lowest (0001) surface energy and small lattice mismatch of wurtzite ZnO crystals with α-sapphire substrates.[3] However, it has been reported that In-doping induced a transition from [001]-oriented NWs to [110]-oriented nanoribbons of ZnO. The transition was attributed to the preferential incorporation of In atoms in the nonpolar [110] direction, which would inhibit the [001] growth of ZnO.[45] In the case of nitrogen-doped ZnO NWs, N atoms possibly play the similar role as In atoms in inducing the transition from [001] to [110] growth of ZnO NWs.

Single-NW-based field-effect transistors (FETs) were used to study the electrical transport properties of NWs. FETs were fabricated by spreading ZnO NWs suspension in alcohol on a SiO_2 (300 nm)/p^+-Si wafers, followed by depositing Ti/Au electrodes on individual NWs by photolithography and e-beam evaporation. Gate voltage was applied to the p^+-Si substrate using the standard global back-gate geometry. Figure 2a shows I_{DS} vs V_{DS} curves of a FET fabricated from a single undoped ZnO NW (bottom inset of Figure 2a). It is clear that all $I_{DS}-V_{DS}$ curves are almost linear, indicating that ohmic contacts are formed between the undoped ZnO NW and Ti/Au electrode. The gate voltage dependence of $I_{DS}-V_{DS}$ curves shows a pronounced gating effect characteristic of n-type conductivity, that is, the conductance of NW increases (or decreases) with increasing (or decreasing) positive V_g. The n-type conduction in undoped ZnO NWs has been attributed to intrinsic donor defects, such as Zn_i and V_O.[43]

Dependence of I_{DS} on V_g at $V_{DS} = 2$ V for sample A is depicted in Figure 2b. On the basis of that, the effective field-effect electron mobility (μ_e) can be estimated by using $g_m = \partial I_{DS}/\partial V_{DS} = \mu C V_{DS}/L^2$, where g_m is the transconductance of an FET, C is the nanowire capacitance, and L is the effective nanowire length between electrodes. $g_m = 1.3 \times 10^{-7}$ A/V is obtained from the linear part of the curve in Figure 2b. The capacitance can be estimated as 1.6×10^{-16} F by $C = 2\pi\varepsilon_0\varepsilon_{SIO_2} L/\ln(4h/d)$, where ε_{SIO_2} is the dielectric constant of SiO_2, h is SiO_2 thickness, and d is NW diameter. The electron mobility μ_e can then be calculated to be 19.5 cm^2/V s at $V_{DS} = 2$ V. Moreover, the electron concentration, n_e, for a quasi-one-dimensional system can be expressed as $n_e = V_{th}C/q\pi(d/2)^2L$, where V_{th} is deduced to be 40 V at $V_{DS} = 2$ V. For sample A, electron concentration is estimated to be 6.1×10^{18} cm^{-3}. The relatively high V_{th} and n_e are due to the relatively thick SiO_2 layer and interface states.[31] According to $\rho = 1/\sigma = 1/nq\mu$, the resistivity of the undoped ZnO NWs is 8×10^{-3} Ω cm. The semilogarithmic plot of I_{DS} vs V_g at a constant $V_{DS} = 2$ V in the left inset in Figure 2a reveals an on/off ratio as large as 10^5.

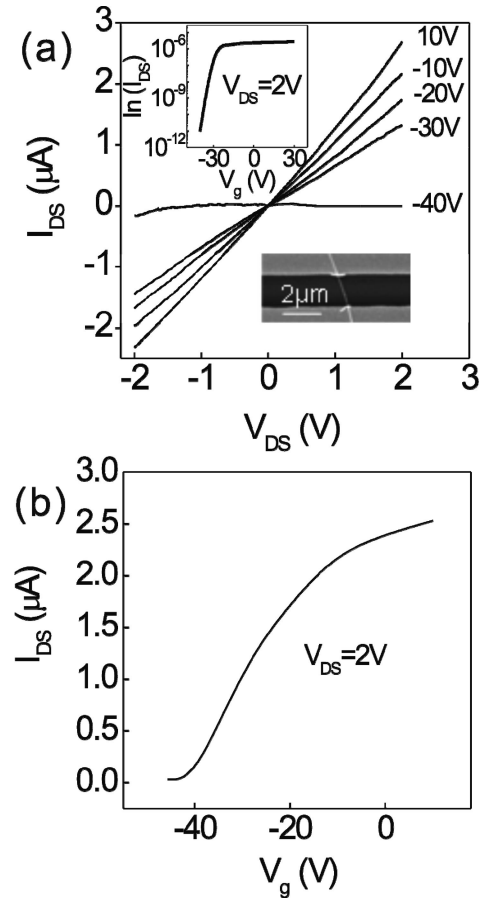

Figure 2. (a) $I_{DS}-V_{DS}$ plots of undoped ZnO NWs (sample A) at different V_g with Ti (100 nm)/Au (20 nm) as electrode. Diameter of the nanowire is 62 nm and effective gate length is about 2.2 μm. The left inset shows ln I_{DS} $-V_g$ plot at $V_{DS} = 2$ V and the right inset is SEM image of the FET. (b) $I_{DS}-V_g$ curve of undoped ZnO NWs.

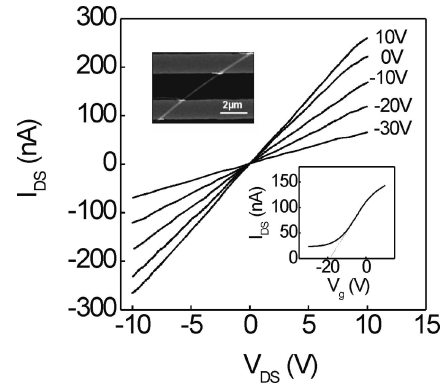

Figure 3. $I_{DS}-V_{DS}$ plots of nitrogen-doped ZnO NWs (sample B, obtained with N_2O:O_2:Ar_2 ratio of 1:20:60) with Ti (100 nm)/Au (20 nm) as electrode. Diameter of the nanowire is 120 nm and effective gate length is 2.8 μm. The right inset shows ln $I_{DS}-V_g$ plot at $V_{DS} = 5$ V and the left inset SEM image of the FET.

We have also measured V_g-dependent transport properties of a NW from sample B (N_2O:O_2:Ar_2 = 1:20:60) using the same FET configuration, and the results are shown in Figure 3. The linear $I_{DS}-V_{DS}$ curves for different V_g confirm the ohmic contact between Ti/Au electrodes and NWs for V_{DS} ranging from −10 to 10 V. Sample B also shows n-type

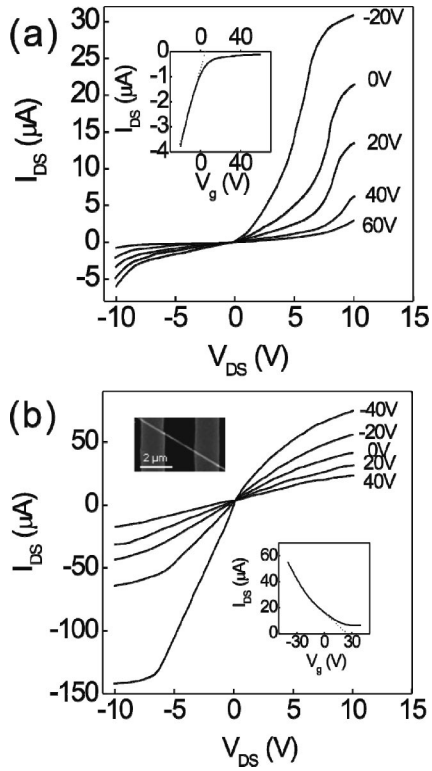

Figure 4. (a) $I_{DS}-V_{DS}$ plots of nitrogen-doped ZnO NWs (sample C, obtained with $N_2O:O_2:Ar_2$ of 2:20:60) at different V_g with Ti (100 nm)/Au (20 nm) as electrode. Diameter of nanowire is 80 nm and effective gate length is 2.1 μm. The left inset shows ln $I_{DS}-V_g$ plot at $V_{DS} = -5$ V. (b) $I_{DS}-V_{DS}$ plots of nitrogen-doped ZnO NWs (sample C) at different V_g with Ni (50 nm) as electrode. Diameter of nanowire is 100 nm and effective gate length is 2.5 μm. The left inset shows an SEM image of FET and the right inset ln $I_{DS}-V_g$ plot at $V_{DS} = 10$ V.

conductivity; however, the I_{DS} of sample B is about 2 orders of magnitude smaller than that of undoped NW (sample A). Similar analysis show the NW has an electron mobility μ_e of 0.39 cm^2/V s, an electron concentration n_e of 8.9×10^{17} cm^{-3}, and a resistivity of 2.9 Ω cm. Comparison to sample A shows that introduction of a small amount of N_2O into the reaction atmosphere leads to a decrease of the electron mobility of ZnO NWs by about 2 orders of magnitude and an increase of the resistivity by almost 3 orders of magnitude. The experimental results show excellent reproducibility, thereby demonstrating N doping can indeed change the electrical properties of ZnO NWs. As discussed above, the undoped ZnO NWs have intrinsic donor defects, such as Zn_i and V_O, which lead to n-type conductivity. When a small amount of nitrogen atoms (acceptors) are introduced into ZnO crystals, they may first partially compensate the intrinsic donor defects and reduce the effective carrier concentration (from 6.1×10^{18} cm^{-3} in sample A to 8.9×10^{17} cm^{-3} in sample B). As a result, sample B remains n-type but with a much higher resistivity.

When N_2O concentration in the reaction atmosphere is further increased ($N_2O:O_2:Ar_2$=2:20:60, sample C), conversion from n-type to p-type conductivity of ZnO NWs is observed. Figure 4a shows the V_g-dependent $I_{DS}-V_{DS}$ curves measured on the FET constructed with a NW from sample C. Remarkably, the V_g-dependent $I_{DS}-V_{DS}$ curves differ distinctively from those of samples A and B. The curves are no longer linear or symmetrical, that is, I_{DS} increases rapidly with increasing positive V_{DS} while maintaining in the OFF state for negative V_{DS}. It indicates that a typical Schottky/rectifying contact exists between the electrodes and ZnO NWs of sample C. Since measurements at larger V_{DS} may help to mitigate the effects of Schottky barriers, we therefore performed measurements in a larger V_{DS} ranging from −10 to 10 V. The $I_{DS}-V_{DS}$ curves show opposite dependence on V_g; that is, the conductance of NWs decreases (or increases) with increasing (or decreasing) positive V_g, which signifies the p-type conductivity in sample C. The formation of rectifying contacts between the electrodes and NWs is consistent with work function alignment between Ti and p-type ZnO.[46]

The $I_{DS}-V_g$ transfer curve obtained from sample C at $V_{DS} = -5$ V is plotted in the inset in Figure 4a. According to the same analysis described above, we obtain a hole mobility (μ_h) of 10.5 cm^2/V s at $V_{DS} = -5$ V, a hole concentration (n_h) of 1.19×10^{18} cm^{-3}, and a resistivity of 0.08 Ω cm. Notably, the hole concentration (1.19×10^{18} cm^{-3} or $\sim 1 \times 10^{10}$ cm^{-1}) and field-effect hole mobility (10.5 cm^2/V s) are significantly larger than those previously reported for phosphor-doped ZnO NWs (2.2×10^7cm^{-1} and 1.7 cm^2/V s).[42] In the phosphor-doped ZnO NWs, it was suggested that the formation of $[P_{Zn}-2V_{Zn}]$ complexes was more favorable rather than P_O, which gave rise to many more defects as evidenced by the enhanced red emission in the PL measurement[42] and thus led to more scattering centers and smaller carrier mobility. Nevertheless, in N-doped ZnO, N atoms should be more favorable to substitute O atoms to form shallow acceptor levels due to the similar atom sizes of N and O. For the same reason, fewer scattering centers would be generated upon N-doping, and thus the hole mobility would be larger.

The electrical and transport properties of nitrogen-doped ZnO NWs (sample C) were also investigated by using Ni electrodes to construct FETs. We expect Ni to form ohmic contact with p-type ZnO NWs because of its high work function (5.15 eV), and Ni has been demonstrated to form ohmic contact with p-type GaN.[31] Figure 4b shows that V_g-dependent I_{DS} vs V_{DS} curves indeed are significantly more linear compared to those obtained on the FET with Ti/Au electrodes (Figure 4a). The V_g-dependent $I_{DS}-V_{DS}$ curves show clear p-type characteristics as expected, confirming again the realization of p-type conductivity in ZnO NWs by nitrogen doping. Using the same analysis as before, we obtain a hole mobility (μ) of 17.2 cm^2/V s, a hole concentration (n_h) of 1.18×10^{18} cm^{-3}, and a resistivity of 0.05 Ω cm. Compared with the calculated electrical parameters with Ti/Au electrodes, the hole mobility derived from the p-ZnO NWs with Ni electrode is a little bit higher, while the resistivity is reduced. It is believed that the low mobility values may be due to the domination of Schottky contact between the p-ZnO NW and Ti/Au electrodes. Therefore, the electrical transport properties derived using the MOSFET equation are more reliable for the p-ZnO NW devices formed

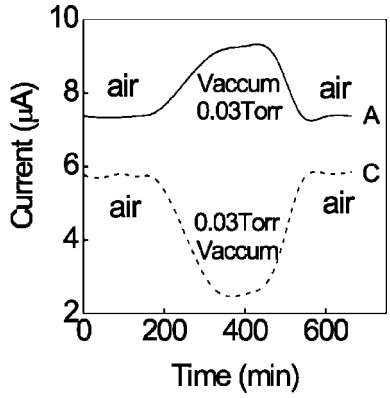

Figure 5. Temporal current responses of ZnO NWs (samples A and C) in air and vacuum.

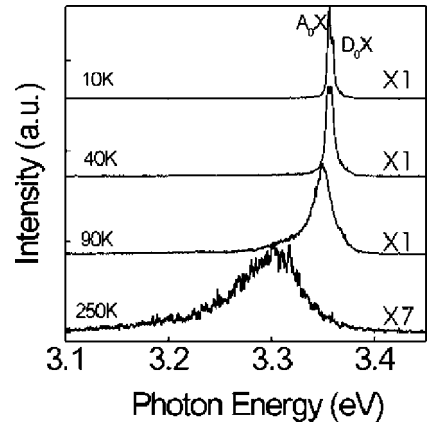

Figure 6. Normalized temperature-dependent PL spectra of the N-doped ZnO NWs (sample C) measured from 10 to 250 K.

with Ni electrodes than that with Ti/Au electrodes.[47–50] Note that we have made and measured at least 15 FETs for each of the samples, and all transport measurements showed excellent reproducibility, ascertaining the results are reliable.

Significantly, for similar hole concentration ($\sim 10^{18}$ cm^{-3}) our p-type ZnO NWs show a hole mobility significantly larger than p-type ZnO thin films (0.03−1 cm^2/V s) doped with N, P, As, Al−N, Ga−N, etc.[35,36,51–54] The results imply that compared to the thin-film counterpart, dopants in ZnO NWs induce fewer carrier scattering centers, and thus NWs are more promising for fabricating high-quality electronic devices. It is important to note that electron mobility decreases drastically from 19.5 in undoped NWs to 0.39 cm^2/V s in lightly nitrogen-doped ZnO NWs (sample B) but regains a high value of 17.2 cm^2/V s in heavily nitrogen-doped sample (sample C). The mobility of the N-doped p-type ZnO NWs is comparable to that of Ga-doped n-type ZnO NWs (16.6 cm^2/V s) at an electron concentration of 10^{19} cm^{-3}.[43] We also note that this hole mobility is higher than Mg-doped p-type GaN NWs (12 cm^2/V s),[31] showing the advantages of our N-doping method. However, the unusual variation of carrier mobility with nitrogen impurity is surprising and not well understood. Nevertheless, our experiments show that carrier mobility depends on carrier concentration; that is, carrier mobility increases with increasing carrier concentration. It suggests that screening of scattering centers by free carriers may play an important role in the transport properties of doped ZnO NWs, as has been reported for Si surfaces,[55] AlGaN-based heterostructures,[56] and ZnO films.[57]

To elucidate the effects of surface conductions, we investigate the electrical and transport properties of both n- and p-type ZnO NWs under different atmospheres. Figure 5 shows the variation of I_{DS} at a constant V_{DS} as the atmosphere is switched between air and vacuum. It can be seen that I_{DS} (or conductance) of sample A increases slowly when the chamber is evacuated to 0.03 Torr but returns to its original value when exposed to air again. The increase and decrease of I_{DS} are attributed to a desorption process in vacuum and an adsorption process in air, respectively. In contrast, sample C shows an opposite behavior; that is, I_{DS} (or conductance) decreases in vacuum. The different variation in the conductance of n- and p-type ZnO NWs toward vacuum can be attributed to adsorption of oxygen on NW surfaces. The adsorbed oxygen molecules would attract electrons from ZnO NWs, leading to reduced electron density in n-type wires but increased hole density in p-type NWs.

Significantly, sample C maintains p-type after storage in air for more than 5 months, although the hole concentration increases by about 1 order of magnitude (see Supporting Information). The gradual increase in hole concentration in p-type ZnO NWs stored in air is believed also due to adsorption of oxygen molecules on NW surfaces. When the sample stored in air is placed in a vacuum of 0.02 Torr, hole concentration is returned to the value close to that before storage, indicating stable p-type conductivity of ZnO NWs was achieved by nitrogen doping. It shows that nitrogen-doped ZnO NWs is much more stable than phosphor-doped NWs. Considering the sizable contribution of surface adsorption to conductivity (~27% for n-type sample A and ~57% for p-type sample C, as shown in Figure 5), surface modification may possibly be an effective method to manipulate the electrical properties of ZnO NWs. The high sensitivity of conductance to surface absorption suggests that ZnO NWs may find applications as gas or chemical sensors.

In order to get more information on the energy level and doping mechanism of nitrogen acceptor in ZnO NWs, we performed temperature-dependent PL measurements. Figure 6 shows the normalized PL spectra of N-doped p-type ZnO NWs (sample C) measured from 10 to 250 K. At high temperature (250 K) the PL spectrum is dominated by free excitons with a maximum intensity at ~3.3 eV; as the temperature decreases, the emission from bound excitons becomes dominant and the emission maxima shift to higher energies. The absence of deep level emissions around 2.5 eV (not shown), which can originate from defects such as Zn_i, V_O, V_{Zn}, and O_{Zn} due to the poor stoichiometry of ZnO,[42] suggests that our p-type ZnO:N has very few intrinsic donor and acceptor defects and that the observed acceptor-related PL emission is due to the nitrogen dopant. The 10 K emission shows two peaks at 3.356 and 3.360 eV, which can be attributed to A_0X and D_0X, respectively,[58] The acceptor energy of the nitrogen dopant was estimated from the A_0X transition using the equation: $E_{eA}(T) = E_g(T) - E_A + k_BT/2$,[59] where E_A and $E_g(T)$ are the acceptor energy level and

band gap, respectively, and k_B is the Boltzmann constant. Since the thermal energy term can be neglected at 10 K, E_A is estimated to be 81 meV, using $E_{eA} = 3.356$ eV and $E_g = 3.437$ eV.[59] The binding energy thus obtained is significantly lower than the value reported for N-doped ZnO thin films (200 meV).[60] However, we point out that the binding energy of phosphor in ZnO NWs (84 meV)[42] is also smaller than the value reported for P-doped ZnO thin films (127 meV, ref 59). We suggest that the difference between the acceptor level in ZnO NWs and that in ZnO films may be attributed to surface effect on dopant energy levels in nanomaterials, although further studies are needed to clarify the findings.

In summary, we demonstrate the growth of high-quality well-aligned single-crystal p-type ZnO NWs on α-sapphire substrates using N_2O as a dopant gas via a simple reactive CVD process. Nitrogen-doped ZnO NWs grow along the [110] direction, distinctly from the [001] growth direction of undoped NWs. Characterization of single ZnO NW FETs shows a transition from n-type conductivity in undoped ZnO NWs to compensated high-resistive n-type, and finally to p-type conductivity in nitrogen-doped NWs with increasing N_2O in the reaction atmosphere. The as-grown p-type ZnO NWs show reproducible and stable electrical properties with a hole concentration of $(1-2) \times 10^{18}$ cm^{-3}, and field effect mobility of 10−17 cm^2 V^{-1} s^{-1}. Surface adsorption, such as oxygen molecules, affects significantly the electrical and transport properties of both undoped and nitrogen-doped ZnO NWs. Temperature-dependent PL spectra of N-doped ZnO NWs show the acceptor-bound-exciton emission, corroborating the p-type conductivity in NWs. Negligible intrinsic defects indicate both undoped and nitrogen-doped ZnO NW arrays have excellent crystalline quality. The success in realizing reliable and stable p-type ZnO NWs should facilitate the fabrication of ZnO NW bipolar devices, in particular electrically driven light-emitting devices.

Acknowledgment. The work was supported by the Research Grants Council of Hong Kong SAR, China (Project No. N_CityU125/05), the strategic Research Grant of the City University of Hong Kong (Project No. 7002121), US Army International Technology Center−Pacific, and the National Basic Research Program of China (973 Program) (Grant No. 2006CB933000 & 2007CB936000).

Supporting Information Available: $I_{DS}-V_{DS}$ plots of nitrogen-doped ZnO NWs. This material is available free of charge via the Internet at http://pubs.acs.org.

References

(1) Huang, Y.; Duan, X.; Wei, Q.; Lieber, C. M. *Science* **2001**, *291*, 630–633.
(2) Lu, W.; Lieber, C. M. *Nat. Mater.* **2007**, *6*, 841–850.
(3) Huang, M. H.; Mao, S.; Feich, H.; Yan, H.; Wu, Y.; Kind, H.; Weber, E.; Russo, R.; Yang, P. D. *Science* **2001**, *292*, 1897–1899.
(4) Qian, F.; Li, Y.; Gradecak, S.; Wang, D.; Barrelet, C. J.; Lieber, C. M. *Nano Lett.* **2004**, *4*, 1975–1979.
(5) Radovanovic, P. V.; Barrelet, C. J.; Gradecak, S.; Qian, F.; Lieber, C. M. *Nano lett.* **2005**, *5*, 1407–1411.
(6) Cui, Y.; Zhong, Z.; Wang, D.; Wang, W. U.; Lieber, C. M. *Nano Lett.* **2003**, *3*, 149–152.
(7) Qin, L. C.; Zhao, X.; Hirahara, K.; Miyamoto, Y.; Ando, Y.; Iijima, S. *Nature* **2000**, *408*, 50.
(8) Wang, N.; Tang, Z. K.; Li, G. D.; Chen, J. S. *Nature* **2000**, *408*, 50.
(9) Pan, Z. W.; Dai, Z. R.; Wang, Z. L. *Science* **2001**, 1947–1949.
(10) Liu, Y. K.; Zapien, J. A.; Shan, Y. Y.; Geng, C. Y.; Lee, C. S.; Lee, S. T. *Adv. Mater.* **2005**, *17*, 1372–1377.
(11) Qian, F.; Gradecak, S.; Li, Y.; Wen, C. Y.; Liber, C. M. *Nano Lett.* **2007**, *5*, 2287–2291.
(12) Lee, S. K.; Kim, T. H.; Lee, S. Y.; Choi, K. C.; Yang, P. *Philos. Mag.* **2007**, *87*, 2105–2115.
(13) Bao, J.; Zimmler, M. A.; Capasso, F. *Nano Lett.* **2006**, *6*, 1719–1722.
(14) Jeong, M.; Oh, B.; Ham, M.; Myoung, J. *Appl. Phys. Lett.* **2006**, *88*, 202105.
(15) Hayden, O.; Agarwal, R.; Lieber, C. M. *Nature* **2006**, *5*, 352–356.
(16) Yang, C.; Zhong, Z.; Lieber, C. M. *Science* **2005**, *310*, 1304–1307.
(17) Javey, A.; Nam, S.; Friedman, R. S.; Yan, H.; Lieber, C. M. *Nano Lett.* **2007**, *7*, 773–777.
(18) Huang, Y.; Duan, X.; Cui, Y.; Lauhon, L. J.; Kim, K.; Lieber, C. M. *Science* **2001**, *294*, 1313–1317.
(19) Zhong, Z.; Wang, D.; Cui, Y.; Bockrath, M. W.; Lieber, C. M. *Science* **2003**, *302*, 1377–1379.
(20) Ahn, J.; Kim, H.; Lee, K.; Jeon, S.; Kang, S.; Sun, Y.; Rogers, J. *Science* **2006**, *314*, 1754–1757.
(21) Yang, C.; Barrelet, C. J.; Capasso, F.; Lieber, C. M. *Nano Lett.* **2006**, *6*, 2929–2934.
(22) Tian, B.; Zheng, X.; Kempa, T. J.; Fang, Y.; Yu, N.; Yu, G.; Huang, J.; Lieber, C. M. *Nature* **2007**, *449*, 885–890.
(23) Cui, Y.; Duan, X.; Hu, J.; Lieber, C. M. *J. Phys. Chem. B* **2000**, *104*, 5213–5216.
(24) Tutuc, E.; Chu, J. O.; Ott, J. A.; Guha, S. *Appl. Phys. Lett.* **2006**, *89*, 263101.
(25) Hsin, C. L.; He, J. H.; Lee, C. Y.; Wu, W. W.; Yeh, P. H.; Chen, L. J.; Wang, Z. L. *Nano Lett.* **2007**, *7*, 1799–1803.
(26) Duan, X.; Huang, Y.; Cui, Y.; Wang, J.; Lieber, C. M. *Nature* **2001**, *409*, 66–69.
(27) Jiang, X.; Xiong, Q.; Nam, S.; Qian, F.; Li, Y.; Lieber, C. M. *Nano Lett.* **2007**, *7*, 3214–3218.
(28) Duan, X.; Huang, Y.; Agarwal, R.; Lieber, C. M. *Nature* **2003**, *421*, 241–245.
(29) Huang, Y.; Duan, X.; Cui, Y.; Lieber, C. M. *Nano Lett.* **2002**, *2*, 101–104.
(30) Qian, F.; Gradecak, S.; Li, Y.; Wen, C. Y.; Liber, C. M. *Nano Lett.* **2007**, *5*, 2287–2291.
(31) Zhong, Z.; Qian, F.; Wang, D.; Lieber, C. M. *Nano Lett.* **2003**, *3*, 343–346.
(32) Li, Y.; Xiang, J.; Qian, F.; Gradecak, S.; Wu, Y.; Yan, H.; Blom, D. A.; Lieber, C. M. *Nano Lett.* **2006**, *6*, 1468–1473.
(33) Li, Y. Q.; Zapien, J. A.; Shan, Y. Y.; Liu, Y. K.; Lee, S. T. *Appl. Phys. Lett.* **2006**, *88*, 013115.
(34) Ronning, C.; Gao, P. X.; Ding, Y.; Wang, Z. L. *Appl. Phys. Lett.* **2004**, *84*, 783–785.
(35) Yuan, G. D.; Ye, Z. Z.; Zhu, L. P.; Qian, Q.; Zhao, B. H.; Fan, R. X.; Perkins, C. L.; Zhang, S. B. *Appl. Phys. Lett.* **2005**, *86*, 202106.
(36) Yuan, G.; Ye, Z.; Zhu, L.; Zeng, Y.; Huang, J.; Qian, Q.; Lu, J. *Mater. Lett.* **2004**, *58*, 3741–3744.
(37) Zhang, S. B.; Wei, S. H.; Zunger, A. *Phys. Rev. B* **2001**, *63*, 075205.
(38) He, H.; Lao, C. S.; Chen, L. J.; Davidovic, D.; Wang, Z. L. *J. Am. Chem. Soc.* **2005**, *127*, 16376–16377.
(39) Yuhas, B. D.; Fakra, S.; Marcus, M. A.; Yang, P. *Nano Lett.* **2007**, *7*, 905–909.
(40) Yuhas, B. D.; Zitoun, D. O.; Pauzauskie, P. J.; He, R. Yang, P. *Angw. Chem., Int. Ed* **2006**, *45*, 420–423.
(41) Fan, H. J.; Fuhrmann, B.; Scholz, R.; Himcinschi, C.; Berger, A.; Leipner, H.; Dadgar, A.; Krost, A.; Christiansen, S.; Gosele, U.; Zacharias, M. *Nanotechnology* **2006**, *17*, S231–S239.
(42) Xiang, B.; Wang, P.; Zhang, X.; Dayeh, S. A.; Aplin, D. P. R.; Soci, C.; Yu, D.; Wang, D. *Nano Lett.* **2007**, *7*, 323–328.
(43) Yuan, G. D.; Zhang, W. J.; Jie, J. S.; Fan, X.; Tang, J. X.; Shafiq, I.; Ye, Z. Z.; Lee, C. S.; Lee, S. T. *Adv. Mater.* **2008**, *20*, 168–173.
(44) Jie, J. S.; Wang, G. Z.; Han, X. H.; Hou, J. G. *J. Phys. Chem. B* **2004**, *108*, 17027–17031.
(45) Fan, H. J.; Barnard, A. S.; Zacharias, M. *Appl. Phys. Lett.* **2007**, *90*, 143116.
(46) Goldberger, J.; Sirbuly, D. J.; Law, M.; Yang, P. *J. Phys. Chem. B* **2005**, *109*, 9–14.

(47) Zhou, C.; Kong, J.; Dai, H. *Appl. Phys. Lett.* **2000**, *76*, 1597–1599.
(48) Liu, X.; Lee, C.; Zhou, C.; Han, J. *Appl. Phys. Lett.* **2001**, *79*, 3329–3331.
(49) Zheng, G.; Lu, W.; Jin, S.; Lieber, C. M. *Adv. Mater.* **2004**, *16*, 1890–1893.
(50) Chang, P.; Fan, Z.; Chien, C.; Stichtenoth, D.; Ronning, C.; Lu, J. G. *Appl. Phys. Lett.* **2006**, *89*, 133113.
(51) Guo, X. L.; Tabata, H.; Kawai, T. *J. Cryst. Growth* **2001**, *223*, 135–139.
(52) Chen, F.; Ye, Z.; Xu, W.; Zhao, B.; Zhu, L.; Lu, J. *J. Cryst. Growth* **2005**, *281*, 458–462.
(53) Ryu, Y. R.; Zhu, S.; Look, D. C.; Wrobel, J. M.; Jeong, H. M.; White, H. W. *J. Cryst. Growth* **2000**, *216*, 330–334.
(54) Joseph, M.; Tabata, H.; Kawai, T. *Jpn. J. Appl. Phys.* **1999**, *38*, L1205–L1207.
(55) Hwang, E. H.; Warma, S. D. *Phys. Rev. B* **2007**, *75*, 073301.
(56) Quang, D.; Tuoc, V.; Tung, N.; Minh, N.; Phong, P. *Phys. Rev. B* **2005**, *72*, 245303.
(57) Studenikin, S. A.; Golego, N.; Cocivera, M. *J. Appl. Phys.* **2000**, *87*, 2413–2421.
(58) Teke, A.; Ozgur, U.; Dogan, S.; Gu, X.; Morkoc, H.; Nemeth, B.; Nause, J.; Everitt, H. O. *Phys. Rev. B* **2004**, *70*, 195207.
(59) Hwang, D.; Kim, H.; Lim, J.; Oh, J.; Yang, J.; Park, S.; Kim, K.; Look, D. C.; Park, Y. S. *Appl. Phys. Lett.* **2005**, *86*, 151917.
(60) Zeuner, A.; Alves, H.; Hofmann, D. M.; Meyer, B. K.; Hoffmann, A.; Haboeck, U.; Strassburg, M.; Dworzak, M. *Phys. Status Solidi* **2002**, *234*, R7–R9.

NL073022T